Title

Accelerated planetesimal growth in self-gravitating protoplanetary discs

Permalink

https://escholarship.org/uc/item/33z6d1k5

Journal

Monthly Notices of the Royal Astronomical Society, 355(2)

ISSN

0035-8711

Authors

Rice, William K
Lodato, G
Pringle, J E
et al.

Publication Date

2004-12-01

Peer reviewed

Accelerated planetesimal growth in self-gravitating protoplanetary discs

W. K. M. Rice,[1]⋆† G. Lodato,[2] J. E. Pringle,[2,3] P. J. Armitage[4,5] and I. A. Bonnell[1]

[1]*School of Physics and Astronomy, University of St Andrews, North Haugh, St Andrews KY16 9SS*
[2]*Institute of Astronomy, Madingley Road, Cambridge CB3 0HA*
[3]*Space Telescope Science Institute, 3700 San Martin Drive, Baltimore, MD 21218, USA*
[4]*JILA, Campus Box 440, University of Colorado, Boulder, CO 80309-0440, USA*
[5]*Department of Astrophysical and Planetary Sciences, University of Colorado, Boulder, CO 80309-0391, USA*

ABSTRACT

In this paper we consider the evolution of small planetesimals (radii $\sim$1–10 m) in marginally stable, self-gravitating protoplanetary discs. The drag force between the disc gas and the embedded planetesimals generally causes the planetesimals to drift inwards through the disc at a rate that depends on the particle size. In a marginally stable, self-gravitating disc, however, the planetesimals are significantly influenced by the non-axisymmetric spiral structures resulting from the growth of the gravitational instability. The drag force now causes the planetesimals to drift towards the peaks of the spiral arms where the density and pressure are highest. For small particles that are strongly coupled to the disc gas, and for large particles that have essentially decoupled from the disc gas, the effect is not particularly significant. Intermediate-sized particles, which would generally have the largest radial drift rates, do, however, become significantly concentrated at the peaks of the spiral arms. These high-density regions may persist for, of order, an orbital period and may attain densities comparable to that of the disc gas. Although at the end of the simulation only $\sim$25 per cent of the planetesimal particles lie in regions of enhanced density, during the course of the simulation at least 75 per cent of the planetesimal particles have at some stage been in a such a region. We find that the concentration of particles in the spiral arms results in an increased collision rate, an effect that could significantly accelerate planetesimal growth. The density enhancements may also be sufficient for the growth of planetesimals through direct gravitational collapse. The interaction between small planetesimals and self-gravitating spiral structures may therefore play an important role in the formation of large planetesimals that will ultimately coagulate to form terrestrial planets or the cores of gas/ice giant planets.

Key words: accretion, accretion discs – planetary systems: formation – planetary systems: protoplanetary discs – stars: pre-main-sequence.

1 INTRODUCTION

The formation of both terrestrial planets and the cores of gas/ice giant planets is thought to occur through the collisional accumulation of planetesimals (Safronov 1972; Wetherill 1990; Weidenschilling & Cuzzi 1993). In the case of gas giant planets, a gaseous envelope is accreted once the core has become sufficiently massive (Lissauer 1993; Pollack et al. 1996). As this must occur while there is still enough gas in the circumstellar disc, and as observations (Haisch, Lada & Lada 2001) suggest that most stars lose their gaseous discs

within $\sim$10[7] yr, it is generally accepted that gas giant planets have to form within $\sim$10[7] yr.

The standard core accretion models of giant planet formation (Pollack et al. 1996; Bodenheimer, O. & J.J. 2000) suggest formation times that could easily exceed disc lifetimes. However, this long formation time-scale problem might be solved in light of the results of recent numerical simulations of the evolution of planetary cores embedded in turbulent accretion discs (Nelson & Papaloizou 2004). These simulations show that cores may actually undergo a random walk through the disc, leading to the suggestion that core migration may significantly accelerate gas giant formation (Rice & Armitage 2003; Alibert, Mordasini & Benz 2004), a possibility initially recognized by Hourigan & Ward (1984).

An additional difficulty in the standard core accretion model is the growth of kilometre-sized planetesimals from, initially, micron-sized dust grains. Within a few scaleheights of the disc midplane,

⋆Present address: Institute of Geophysics and Planetary Physics, University of California, Riverside, CA 92521, USA.
†E-mail: ken.rice@ucr.edu

the pressure gradient in the circumstellar disc tends, for standard disc geometries, to be negative and causes the gas to orbit with sub-Keplerian velocities. The dust, which is not affected by the gas pressure gradient, and the gas therefore orbit with different velocities and the resulting drag force causes the dust grains to drift inwards at a rate that depends on their size (Weidenschilling 1977; Takeuchi & Lin 2002). For small sizes, the dust grains are essentially coupled to the disc gas and the radial drift velocity is consequently small. For large sizes, the grains are decoupled from the gas, move in nearly Keplerian orbits, and again have small radial drift velocities. Particles with intermediate sizes can, however, have large inward radial velocities. Although the exact size range depends on the circumstellar disc properties, the maximum radial velocity may easily exceed 10^3 cm s^{-1} and is normally thought to occur for objects with sizes between 1 cm and 1 m (Weidenschilling 1977).

Although the differential radial velocity is a crucial part of the grain growth, as larger objects grow by sweeping up smaller objects (e.g. Safronov 1972; Weidenschilling & Cuzzi 1993), if the maximum radial velocity is too high these objects may drift inwards before they can become large enough to decouple from the disc gas. Together with the inward radial drift, the larger grains may also settle towards the midplane (Goldreich & Ward 1973; Garaud, Barriére-Fouchet & Lin 2004), producing a thin, dense dust layer (note, however, that the presence of turbulence in the disc can prevent the dust settling, see Stone et al. 1996). This layer may become self-gravitating and, if sufficiently unstable, could produce kilometre-sized objects directly via gravitational collapse (Goldreich & Ward 1973). This, however, requires extremely small random dust velocities ($\sim$10 cm s^{-1}), which may be difficult to achieve (Weidenschilling & Cuzzi 1993; Cuzzi, Dobrovolski & Champney 1993). Even if such small random velocities are possible, if objects are to grow via gravitational collapse, any increase in the random velocities has to be lost very rapidly (Gammie 2001; Rice et al. 2003a).

An alternative mechanism for the formation of gas giant planets, which does not require the initial growth of a core, is that the gas itself may become unstable, producing gravitationally bound gaseous protoplanets (Boss 1998, 2000). This again requires that the gas be cold and that it remain 'almost isothermal' (Pickett et al. 1998, 2000) or, equivalently, that any cooling mechanism is extremely efficient (Gammie 2001; Rice et al. 2003a; Johnson & Gammie 2003). Furthermore, some simulations of fragmenting protoplanetary discs suggest that, at best, this mechanism may be able to produce only the most massive ($>$5 Jupiter masses) gas giant planets (Rice et al. 2003b).

We study here the influence of the development of gravitationally unstable spiral modes on the planet formation mechanism via core accretion (see also Haghighipour & Boss 2003a). Although it is possible that the conditions required for disc fragmentation may never be met (Pickett et al. 2000), it is quite likely that protostellar discs are self-gravitating in their early stages (e.g. Lin & Pringle 1990; Lodato & Bertin 2001). If so, the disc then becomes susceptible to the growth of non-axisymmetric spiral structures which can transport angular momentum very efficiently (e.g. Lodato & Rice 2004). In the presence of such spiral structures, the gas pressure gradient, which can be large, changes from positive on one side of the structure to negative on the other, resulting in both super- and sub-Keplerian gas velocities. The gas drag force then causes dust grains to drift both radially inwards and outwards, depending on whether the local gas velocity is super-Keplerian or sub-Keplerian (Haghighipour & Boss 2003a,b). The net effect is that the dust drifts towards the density maxima, where the pressure gradient is zero

(Haghighipour & Boss 2003a). A similar effect would occur in the presence of any coherent and long-lived density enhancement. Previous work (Godon & Livio 2000; Klahr & Bodenheimer 2003) has considered how vorticies may influence embedded particles. The formation of such vorticies is, however, still a matter of some debate.

In this paper we present the results of three-dimensional, global simulations of self-gravitating accretion discs in which we include both gas and dust, coupled via a drag force (Whipple 1972; Weidenschilling 1977). The gaseous disc is maintained in a state of marginal gravitational instability, achieved by letting the disc cool down (through a simple parametrization of the cooling function; Gammie 2001 and Rice et al. 2003a). In this way a quasi-steady spiral structure develops in the disc and is maintained during several dynamical time-scales. We are therefore able to follow the process of concentration of the planetesimals in the spiral arms. We have performed several simulations, considering planetesimals of different sizes. We find that, for a given size range, the planetesimals are indeed able to reach high concentrations, in some regions attaining densities comparable to the gas. This could significantly enhance the coagulation of planetesimals into larger bodies, by increasing the planetesimal collision rates and/or by making the planetesimal sub-disc become gravitationally unstable (Youdin & Shu 2002; Youdin & Chiang 2004).

This paper is organized as follows. In Section 2 we summarize the basic features of the coupled dynamics of a two-component (gas and planetesimals) disc, including a description of the relevant drag forces. In Section 3 we describe the simulation code that we have used and the numerical setup. In Section 4 we describe our results. In Section 5 we draw our conclusions.

2 GAS–PLANETESIMAL DISC DYNAMICS

We consider a system comprising two interpenetrating discs: a 'gas' disc, that is evolved using the standard hydrodynamical equations of motion, and a 'planetesimal' disc, that is considered as a collection of test particles evolved under the influence of gravitational and drag forces alone. Both the 'gas' disc and the 'planetesimal' disc rotate around a central protostar of mass $M_\star$, which we take to be equal to 1 M$_\odot$. The term 'planetesimal' is generally used to refer to particles that have decoupled from the disc gas. Although the particles we consider here are still coupled to the gas, we use this term because, as we will discuss later, the particles we consider are clearly too large to be regarded as dust grains.

To illustrate the basic dynamical ingredients of our model, and to introduce the relevant physical quantities, let us consider first the simple case of a smooth, axisymmetric, non-self-gravitating disc. We define the Keplerian velocity, V_K, around the star at a distance R by

$$V_K^2 = GM_\star/R. \tag{1}$$

The gas disc is characterized by a surface density profile $\Sigma(R)$, a temperature profile $T(R)$ and a pressure profile $P(R)$. The gas sound speed is defined as

$$c_s^2 = \frac{\partial P}{\partial \rho}, \tag{2}$$

where ρ is the gas volume density. Let $\mathbf{v}$ and $\mathbf{v}_p$ be the velocities of the gas and of the planetesimals, respectively. In centrifugal equilibrium the azimuthal component of the gas velocity v_ϕ is given by

$$v_\phi^2 = V_K^2 + \left(\frac{d \ln \rho}{d \ln R}\right) c_s^2 = V_K^2(1 + \gamma), \tag{3}$$

where $\gamma \equiv (\mathrm{d}\ln\rho/\mathrm{d}\ln R)c_\mathrm{s}^2/V_\mathrm{K}^2$, is a measure of the importance of thermal effects in the disc. For most disc models, the density ρ decreases with radius, so that $\gamma < 0$ and v_ϕ is generally sub-Keplerian. If the gas disc is in vertical hydrostatic equilibrium, its aspect ratio is given by

$$\frac{H}{R} \approx \frac{c_\mathrm{s}}{V_\mathrm{K}} = \left|\frac{\mathrm{d}\ln\rho}{\mathrm{d}\ln R}\right|^{-1/2}\sqrt{|\gamma|}. \tag{4}$$

The planetesimals, on the other hand, are not affected by pressure forces and, in centrifugal equilibrium therefore orbit at the Keplerian velocity V_K. Let $\boldsymbol{u}$ be the relative velocity between the gas and the planetesimals. We assume that the gas and the planetesimals are coupled through a drag force, as described by Weidenschilling (1977) and Whipple (1972). The drag force is given by

$$\boldsymbol{F}_\mathrm{D} = -\frac{1}{2}C_\mathrm{D}\pi a^2\rho u^2\hat{\boldsymbol{u}}, \tag{5}$$

where $u = |\boldsymbol{u}|$, $\hat{\boldsymbol{u}} = \boldsymbol{u}/u$, a is the mean radius of the planetesimals and C_D is the drag coefficient, given by

$$C_\mathrm{D} = \begin{cases} \dfrac{8}{3}\dfrac{c_s}{u} & a < 9\lambda/4 \\[2mm] 24R_\mathrm{e}^{-1} & R_\mathrm{e} < 1 \\[2mm] 24R_\mathrm{e}^{-0.6} & 1 < R_\mathrm{e} < 800 \\[2mm] 0.44 & R_\mathrm{e} > 800. \end{cases} \tag{6}$$

The drag regime where $a < 9\lambda/4$ is generally called the Epstein regime, whereas the other three regimes define the Stokes drag. In the previous expression, R_e is the Reynolds number, defined below in equation (9) and λ is the mean-free path of the gas particles. Assuming the gas to be made mainly of molecular hydrogen, this is given by

$$\lambda = \frac{m_{\mathrm{H}_2}}{\rho A} \approx \frac{4\,10^{-9}}{\rho}\mathrm{cm}, \tag{7}$$

where in the last expression the gas density ρ is evaluated in cgs units, m_{H_2} is the mass of the hydrogen molecule, and A is its cross-section, i.e.

$$A = \pi a_0^2 \approx 7\,10^{-16}\,\mathrm{cm}^2, \tag{8}$$

where a_0 is the mean radius of the hydrogen molecule (see Supulver & Lin 2000).

The Reynolds number R_e is given by

$$R_\mathrm{e} = \frac{2a\rho u}{\eta}, \tag{9}$$

where $\eta = \rho\nu$ is the gas viscosity. For collisional viscosity, we have

$$\eta = \frac{\rho c_s\lambda}{2}. \tag{10}$$

We can therefore write

$$R_\mathrm{e} = 4\left(\frac{a}{\lambda}\right)\left(\frac{u}{c_s}\right). \tag{11}$$

For the disc properties and particle sizes that we will consider here, the Mach number rarely exceeds unity and the Reynolds number generally falls in the range $1 < R_\mathrm{e} < 800$. Only in the inner regions of the disc, where $\boldsymbol{u}$ is largest, does the Mach number exceed unity and the Reynolds number exceeds 800.

Another important quantity is the 'stopping time' t_e, where

$$t_\mathrm{e} = \frac{m_\mathrm{p}u}{|F_\mathrm{D}|}. \tag{12}$$

Here $m_\mathrm{p} = 4\pi\rho_\mathrm{s}a^3/3$, is the mass of the planetesimals and ρ_s is the internal density of the planetesimals (throughout the paper, we take $\rho_\mathrm{s} = 3\,\mathrm{g\,cm}^{-3}$). With the previous definitions, we have

$$\frac{t_\mathrm{e}}{t_\mathrm{d}} = \frac{8}{3C_\mathrm{D}}\left(\frac{\rho_\mathrm{s}}{\rho}\right)\left(\frac{V_\mathrm{K}}{u}\right)\left(\frac{a}{R}\right), \tag{13}$$

where $t_\mathrm{d} = \Omega_\mathrm{K}^{-1} = R/V_\mathrm{K}$ is the local dynamical time-scale. The smaller the $t_\mathrm{e}/t_\mathrm{d}$ value, the more strongly the planetesimals are coupled to the gas. It is well known (Weidenschilling 1977) that the gas–planetesimal interaction through the drag force causes the planetesimals to migrate in the direction of increasing pressure (i.e. inward, for a smooth, axisymmetric disc). The migration rate depends on the particle size and there is a range of particles sizes (the extent of which depends on the gas disc properties) that are characterized by a relatively large radial drift.

Consider, as an illustration, the average structure of one of the gas discs obtained from the numerical simulations of self-gravitating discs by Lodato & Rice (2004). On average, these discs are characterized by a power-law surface density profile, $\Sigma \propto R^{-1}$, and by an approximately flat profile, with a value of order unity, of the axisymmetric gravitational stability parameter Q (Toomre 1964)

$$Q = \frac{c_\mathrm{s}\kappa}{\pi G\Sigma}. \tag{14}$$

In the previous expression κ is the epicyclic frequency, that, for the nearly Keplerian discs considered here, is roughly equal to the orbital frequency Ω, to order H^2/R^2. The disc extends from $R_\mathrm{in} = 0.25$ au to $R_\mathrm{out} = 25$ au. The total disc mass is $M_\mathrm{disc} = 0.25\,\mathrm{M}_\odot$. The profile of Q essentially determines the pressure structure in the disc. We have then that $c_\mathrm{s} \propto R^{1/2}$, $H/R \propto R$ and $\rho \propto R^{-3}$.

We can therefore estimate the radial drift velocity of planetesimals in such a disc, using standard techniques (Weidenschilling 1977). The results are shown in Fig. 1, where the left panel shows the radial drift velocity u_r in units of the local Keplerian velocity. Equivalently, defining the drift time-scale $t_\mathrm{r} = R/u_\mathrm{r}$, we have $u_\mathrm{r}/V_\mathrm{K} = t_\mathrm{d}/t_\mathrm{r}$, so that the left panel of Fig. 1 also shows a measure of the drift time-scale compared to the dynamical time-scale. In the right panel of Fig. 1 we also show t_r in years. It can be seen that for the assumed average gas disc properties, the largest radial drift would occur for planetesimals with sizes in the range between 10 and 100 cm. It should, however, be kept in mind that these results refer to the azimuthally averaged structure of the disc. Actually, the self-gravitating gas disc is characterized by a spiral structure, with alternating regions of high and low gas densities (see Fig. 2). Equation (3) then readily shows that the gas velocity changes from sub-Keplerian through super-Keplerian, when moving across one arm of the spiral structure. The drag force causes the planetesimals to drift towards regions of higher pressure (and hence of higher density), so we expect that the planetesimals tend to concentrate very fast around the maxima of the gas density (see also Haghighipour & Boss 2003a). The results described above then suggest, for the disc we are considering here, that this effect is maximal for planetesimals with sizes between 10 and 100 cm.

The expected drift time-scale, in such structured discs, is going to be smaller than in a smooth disc. In fact, in a smooth, power-law disc the pressure gradient is $\nabla P \sim P/R$, while in a disc with a spiral structure (characterized by a typical scale $\sim H$) the pressure gradient is of order $\nabla P \sim P/H$. The increased pressure gradient decreases the drift time-scale by a factor H/R. The drift time-scale is decreased by further factor H/R because the planetesimals have to move
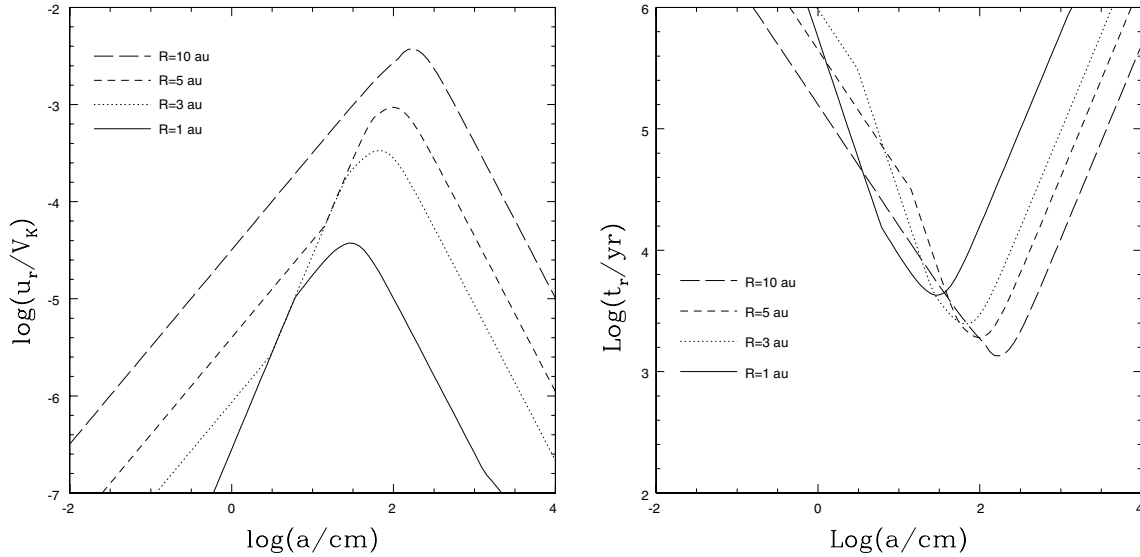
Figure 1. Left panel: radial drift velocity (in units of the local Keplerian velocity) as a function of planetesimal size for the assumed disc structure. Right panel: radial drift time-scale as a function of planetesimal size. The curves refer to four different locations in the disc: solid line, 1 au; dotted line, 3 au; dashed line, 5 au; long-dashed line, 10 au.
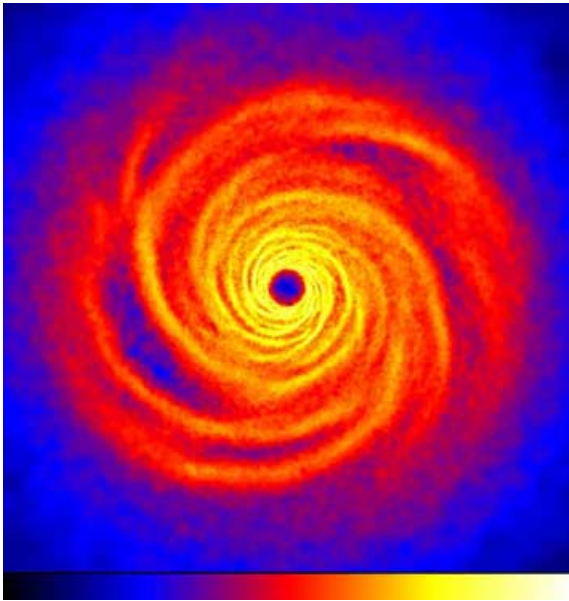

Figure 2. Surface density structure of a self-gravitating disc with $M_{disc} = 0.25\,M_{\odot}$ (the central star mass is $M_{\star} = 1\,M_{\odot}$). The spiral structure is a quasi-steady feature lasting for at least several thermal time-scales. The panel shows the logarithm of the surface density Σ with the scale covering $1 < \log(\Sigma/\mathrm{g\,cm}^{-2}) < 4.7$. The size of the box is 50 au across.

only a distance of order H to reach the density maxima. We therefore expect a significant concentration of the planetesimals around the gas density maxima to take place over a time-scale a factor $(H/R)^2 \sim 0.01$ smaller than that displayed in Fig. 1, becoming therefore comparable with the dynamical time-scale in the most favourable cases. By inspection of the right panel of Fig. 1, we also obtain that for particles with sizes between $\sim$10 and $\sim$1000 cm, we need only run our simulation for about 100 yr to follow the effect of radial drift on the planetesimal subdisc.

3 NUMERICAL SIMULATIONS

3.1 Smoothed particle hydrodynamics

The three-dimensional gaseous disc used in these simulations is modelled using smoothed particle hydrodynamics (SPHs), a Lagrangian hydrodynamics code (see Benz 1990; Monaghan 1992). The gas disc consists of 250 000 SPH particles, each of which has a mass and an internal energy (temperature). Each particle also has a smoothing length that is allowed to vary with time to ensure that the number of neighbours (SPH particles within two smoothing lengths) remains $\sim$50. These neighbouring particles are used to determine the density which, together with the internal energy, is used to compute the pressure. The central star is modelled as a point mass on to which gas particles may accrete if they approach to within the sink radius (e.g. Bate, Bonnell & Price 1995), here taken to be 0.25 au. Both the central point mass and the gas particles use a tree to determine gravitational forces, and to determine the gas particle neighbours.

The small planetesimals are modelled using an additional type of particle. These particles are, as far as the gas simulation is concerned, massless (i.e. in these simulations we neglect the self-gravity of the planetesimal disc and the back reaction of the drag force on the gas). They experience only gravitational forces (from the central star and from the disc gas) and are coupled to the disc gas via a drag force. As discussed in Section 2 the drag force depends on the particle size, the local gas density and on the local gas velocity. To determine the drag force coefficient also requires the gas sound speed which is calculated using the local gas internal energy. The gravitational force on these test particles is computed by including them in the tree. This also determines their nearest gas neighbours. To ensure that the number of gas neighbours remains $\sim$50, the test particles also have a smoothing length that is allowed to vary with time. These neighbouring particles are then used to calculate the gas density, velocity and internal energy at the location of each test particle using the standard SPH formalism (see Monaghan 1992). The exact value of the drag force is then determined by specifying the planetesimal size. In each simulation performed here, we use

125 000 test particles to represent a planetesimal disc which we assume contains particles of a single size.

An additional saving in computational time is made by using individual particle time-steps (Bate et al. 1995) with the time-steps for each particle limited by the Courant condition and by a force condition (Monaghan 1992). As will be discussed in more detail in the following sections, the gas disc is assumed, in the absence of any cooling mechanism, to have an adiabatic equation of state with an adiabatic index of $\gamma = 5/3$. The gas disc is initially evolved, in the absence of test particles, by imposing a cooling term which is chosen such that the disc ultimately settles into a quasi-steady, self-gravitating state. The test particles are then added and the simulation is evolved for an additional outer rotation period.

3.2 Self-gravitating gas disc simulations

In this work we use the results of the numerical simulations by Lodato & Rice (2004) of the dynamics of self-gravitating gas discs as an input for our two-component gas–planetesimals disc simulations.

It is well known that the onset of gravitational instabilities in the disc is determined by the value of the parameter Q, defined in equation (14). If Q is smaller than a threshold value of order unity, the disc quickly develops a spiral structure on the dynamical time-scale. The presence of the spiral influences strongly the thermal evolution of the disc, in that it provides a source of effective heating. As Q is proportional to the thermal speed c_s, in the absence of any cooling Q would rapidly become relatively large and the spiral structure would vanish. However, if some cooling is present, a self-regulated state can be achieved where the heating provided by the spiral structure balances the external cooling, leading to a long-lasting spiral.

These processes have been recently explored numerically by Lodato & Rice (2004) (see also Gammie 2001), who have performed global, three-dimensional simulations of the evolution of self-gravitating discs. They imposed a cooling of the form

$$\frac{\mathrm{d}U}{\mathrm{d}t}\bigg|_{\mathrm{cool}} = -\frac{U}{t_{\mathrm{cool}}}, \tag{15}$$

where U is the internal energy of the gas and the cooling time-scale is taken to be simply proportional to the dynamical time-scale, $t_{\mathrm{cool}} = \beta \Omega^{-1}$. For very rapid cooling time-scales ($\beta \lesssim 3$) the self-gravitating disc undergoes fragmentation (Gammie 2001; Rice et al. 2003a). In this work we have taken $\beta = 7.5$, giving a cooling time that should not, and indeed does not, lead to fragmention.

The simulations by Lodato & Rice (2004) indeed show the effectiveness of the self-regulation process. The disc extends from 0.25 to 25 au, and is characterized initially by a surface density profile $\Sigma \propto R^{-1}$ and a temperature profile $T \propto R^{-1/2}$. The exact surface density is determined by specifying a total disc mass, and the temperature is determined by specifying that the Toomre Q parameter has an initial value of 2 at the outer edge of the disc. The temperature profile, however, is rapidly modified by the competing heating and cooling processes operating in the disc, as discussed above. At the end of the simulations a self-regulated state is achieved with an almost constant profile of Q, with a value close to unity. The spiral structure obtained in this way is a quasi-steady feature lasting for at least several thermal time-scales (i.e. at least until the end of the simulations). Fig. 2 shows the final disc structure for a disc whose total mass is $M_{\mathrm{disc}} = 0.25\,\mathrm{M}_\odot$. The image shows the logarithm of Σ, with a colour scale covering $1 < \log(\Sigma/\mathrm{g\,cm^{-2}}) < 4.7$.

The spiral structure transports angular momentum in the disc and therefore promotes the accretion process. This leads also, in some cases, to a steepening of the surface density profile. This process

however occurs on the much longer 'viscous' time-scale, so that the final profile of Σ is only slightly modified with respect to the initial one (see Lodato & Rice 2004).

3.3 Numerical setup

We initially evolve the gas disc in the absence of any test particles, as described in the previous section. After ~ 6 orbital periods at the outer edge of the disc (i.e. after ~ 800 yr), a quasi-steady, self-regulated state is reached. We then introduce the planetesimals and evolve the simulation as described in Section 3.1 for roughly one more outer orbital period (i.e. ~ 125 yr).

To cover a wide range of planetesimal sizes we have considered separately planetesimal sizes of 50 and 1000 cm. Based on the results of Section 2, we expect the 50-cm sized planetesimal to have the largest radial drift. For smaller planetesimal sizes (e.g. 1 cm) we expect the acceleration owing to the drag force to be very large, resulting in extremely long computation times. However, for such small planetesimals, we expect the drag to be so large that their structure will closely match that of the gas. In addition to the 50- and the 1000-cm cases, we have also performed one simulation in which no drag force was included, so as to provide a direct measure of the effect of gas drag on the evolution of the planetesimals.

The planetesimal disc initially extends from $R = 2$ to $R = 20$ au. The surface density profile of the planetesimals Σ_p was taken to be proportional to R^{-1}. As we neglect the self-gravity of the planetesimals and the back reaction of the drag force on the gas, the actual value of the planetesimal disc surface density does not influence the results of the simulations (the planetesimal SPH particles are just a 'tracer' of the evolution of the solid bodies in the gas disc). However, to present illustration values in the analysis of our results, we will assume that the initial ratio of the planetesimal to gas surface densities is 0.01 in all cases.

Initially all the planetesimals are located in the $z = 0$ plane. However, during the simulation, the random motions induced by the gravitational instabilities rapidly stir the planetesimal disc up, so that eventually it acquires a finite thickness H_p slightly smaller than the gas disc thickness H.

4 RESULTS

Fig. 3 shows the surface density structure of the planetesimal discs, one outer orbital time after the introduction of the planetesimals in the simulations (i.e. after ~ 125 yr). At this stage, most of the disc has evolved for several dynamical time-scales, so that any initial transient features have disappeared. The figure refers to the cases where the planetesimal sizes were 50 cm (left panels) and 1000 cm (right panels). The upper panels show the logarithm of the surface density Σ_p (to have a direct comparison with Fig. 2, the surface densities have been multiplied by 100 and the same colour scale has been used). The bottom panels show the ratio Σ_p/Σ of the planetesimal and gas surface densities. The colour scales in the latter plots are exactly the same for the two different planetesimal sizes and covers the range $0.004 < \Sigma_p/\Sigma < 0.04$.

These plots clearly show how the planetesimal evolution changes with changing planetesimal size. As expected, the 50-cm planetesimals are strongly influenced by the gas drag and display a spiral pattern with very thin spiral arms, indicating that the planetesimals are concentrated at the bottom of the potential. The effect is reduced in the 1000-cm case, where the spiral structure in the planetesimal disc is similar to that of the gas disc, indicating that the planetesimals are pushed into the spirals mainly because of the gravitational
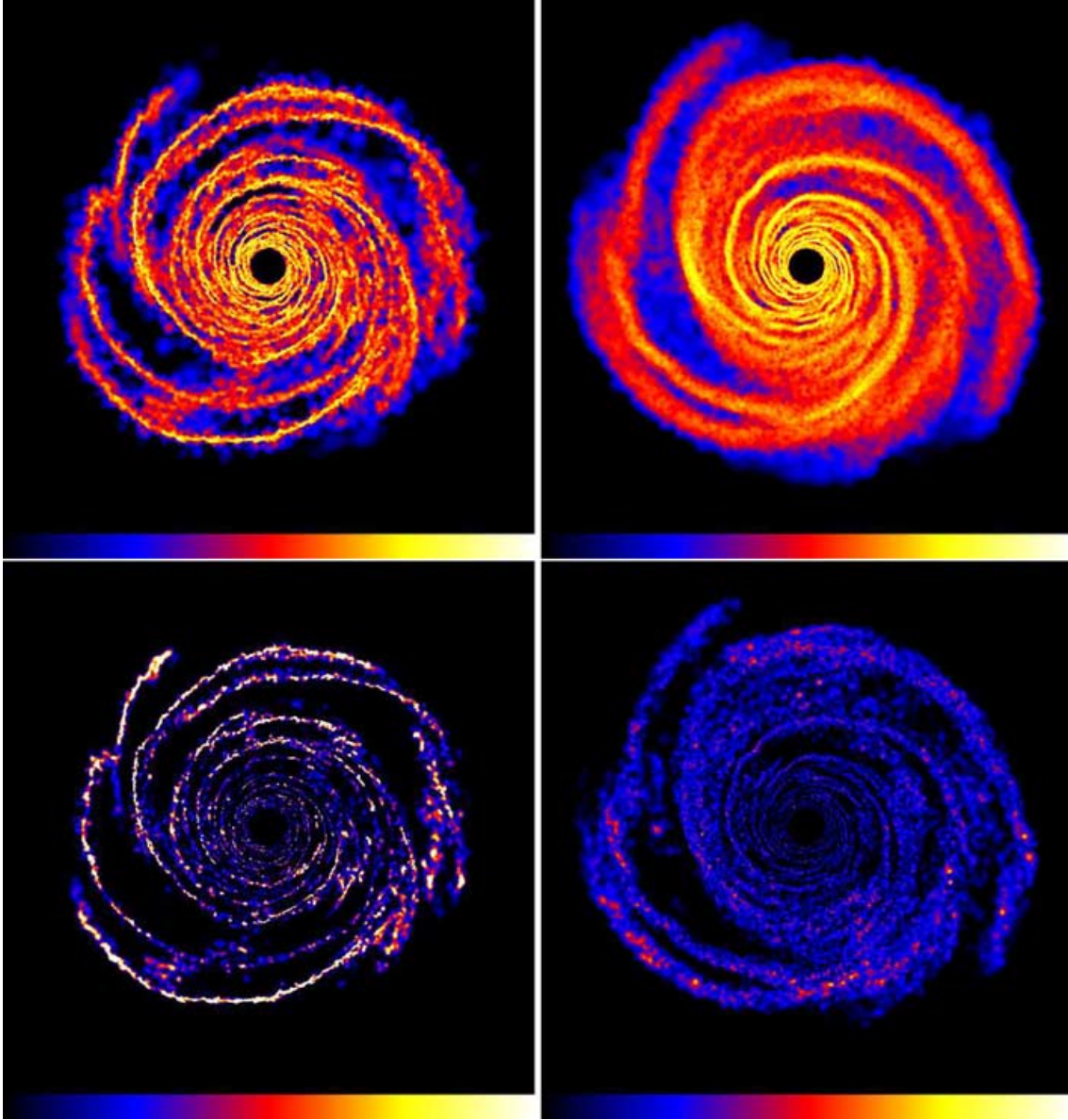
Figure 3. Surface density structure of the planetesimal discs after one outer orbital time. The upper panels show Σ_p, for the 50-cm planetesimals (left panel) and for the 1000-cm planetesimals (right panel). The surface densities have been multiplied by 100 and the colour scaling is the same as in Fig. 2, in order to have a direct comparison with the gas surface density structure. The size of the box displayed is also the same as in Fig. 2. The bottom panels show the ratio Σ_p/Σ for the two cases (the colour scales of these panel are the same in the two cases and cover $0.004 < \Sigma_p/\Sigma < 0.04$). If the gas and planetesimals respond in the same way to the gravitational instabilities, the density ratio would be uniform through the disc, so that any non-uniformity in the bottom panels is a direct measure of the concentration effect on the planetesimals caused by the combination of gas gravity and drag force. The planetesimal tend to concentrate in clumpy regions along the spiral arms, where the minima of the gravitational potential are located. The effect is particularly evident for planetesimal size of 50 cm, for which Σ_p/Σ can be enhanced by more than a factor of 50.

field (note that as the planetesimals have no pressure support, we expect the spiral arms to be slightly thinner even if no drag force is introduced). A similar structure, with relatively broad spiral arms, was indeed also seen in the simulation with no drag force.

The bottom panels in Fig. 3 show how the concentration of planetesimals is modified by the combined effect of gas drag and gravity. If the gas and planetesimals respond in the same way to the gravitational instabilities, the density ratio would be uniform through the disc, so that any non-uniformity in the bottom panels is a direct measure of the concentration effect on the planetesimals caused by the combination of gas gravity and drag force. Clearly, the 50-cm

planetesimal reach a much higher concentration compared to the 1000-cm case. At the end of the simulation Σ_p/Σ has increased by a factor ~ 3 for the 1000-cm case, while in the 50-cm case the maximum increase can be as high as ~ 50, in some regions therefore reaching surface densities comparable to that of the gas.

Fig. 4 shows a histogram of the distribution of planetesimal volume densities, ρ_p, for both the 50- and 1000-cm particles (left panel), and a histogram of the distribution of gas volume densities, ρ, scaled down by two orders of magnitude for a direct comparison with the planetesimal density (right panel), at the end of the simulations. In both panels N_{tot} is the total number of particles of the type
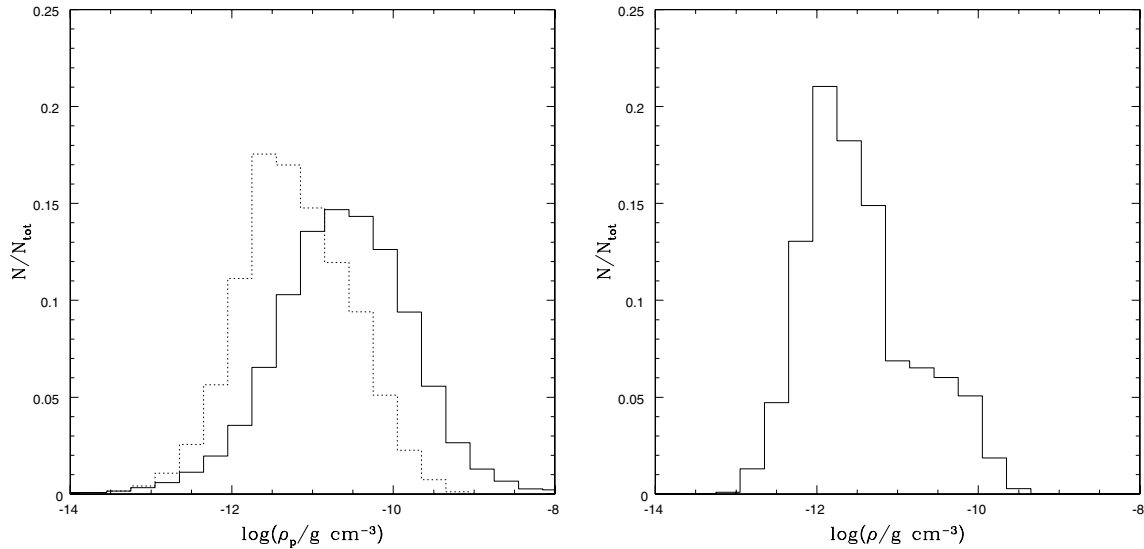
Figure 4. Left panel: volume density distribution of the planetesimal for the two different sizes considered (solid line, 50 cm; dotted line, 1000 cm), at the end of the simulation. Note that the particular shape of the density distribution is not very meaningful, as it depends on the initial surface density distribution that we assume. What is interesting is that, starting from the same initial density distribution, at the end of the simulation the 50-cm sized planetesimals can reach densities at least one order of magnitude larger than the 1000-cm case. Right panel: corresponding gas density distribution at the end of the simulation, scaled down by two orders of magnitude for a direct comparison with the planetesimal density.

being considered. The planetesimal volume densities were determined by assuming, as mentioned earlier, that the initial planetesimal to gas surface density ratio was 0.01. The distribution for the 50-cm planetesimals (solid line – left panel) shows a tail at high densities extending to more than an order of magnitude above the 1000-cm planetesimals (dotted line – left panel). The distribution of gas volume densities (right panel) is also similar to that of the 1000-cm particles, again illustrating that the 1000-cm particles are more strongly influenced by the gravitational potential than by the drag force. The concentration of planetesimals is further illustrated in Fig. 5 which shows the distribution of the ratio of the planetesimal volume density to the gas volume density. This shows that the volume density of the 50-cm planetesimals (solid line) may increase to a value similar to the gas density. The volume density ratio for the 1000-cm particles (dotted line), on the other hand, barely exceeds 0.1 and in most regions has a value below 0.05. Given an 'unperturbed' density ratio of 0.01, this means that the volume density of the 1000-cm particles is almost never enhanced by more than a factor of 10. These results confirm our expectations that for the planetesimals with the largest expected radial drift, the combined effect of gas drag and spiral structure induced by self-gravity leads to a significant concentration of the planetesimals along the spiral arms.

Fig. 6 shows how the volume density, as seen by a representative planetesimal located at $\sim$8 au, varies with time. The left and the right panels display the results for the 50 and the 1000-cm cases, respectively. The solid line shows the planetesimal volume density, while the dotted line shows the corresponding gas volume density. The differences between the two cases are striking also in this case. The planetesimal density for the 1000-cm particles essentially follows closely the gas density, with relatively small variations, and oscillates between high and low values as the planetesimal goes in and out of the regions of enhanced gas density (the spiral arms). In the 50-cm case, the planetesimal density reaches extremely high values becoming comparable to the gas density when the planetesimal moves into a spiral arm. The planetesimal density can also
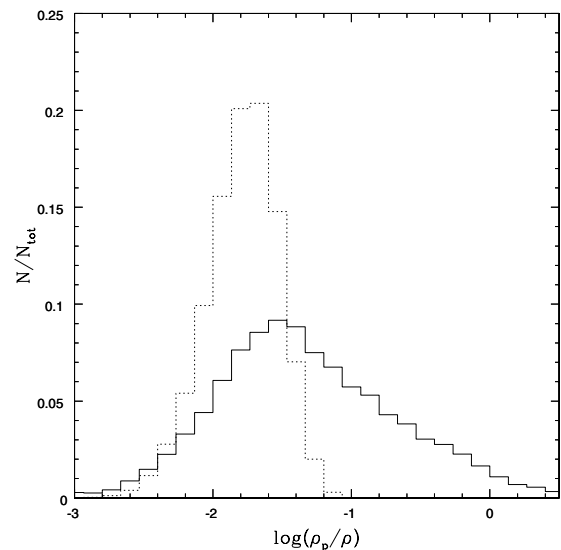

Figure 5. Distribution of volume density ratios (planetesimal/gas) for the two different sizes considered (solid line, 50 cm; dotted line, 1000 cm) at the end of the simulation. While the planetesimal/gas density ratio is generally smaller than 0.05 for the 1000-cm case (i.e. the concentration enhancement is smaller than 5), in the 50-cm case it can reach values of the order of unity (concentration enhancement $\sim$100).

remain high for as long as $\sim$20 year, comparable to the dynamical time-scale at 8 au.

To summarize, Fig. 5 shows that at a given time a significant fraction of the 50-cm planetesimals have a large concentration (say, $\rho_p/\rho > 0.1$). On the other hand, Fig. 6 shows that a given particle spends only a fraction of the total simulation at high ρ_p/ρ. This suggest that the total fraction of planetesimals which at some stage during the run have a large ρ_p/ρ is actually larger than the corresponding fraction taken at a given time. To estimate this
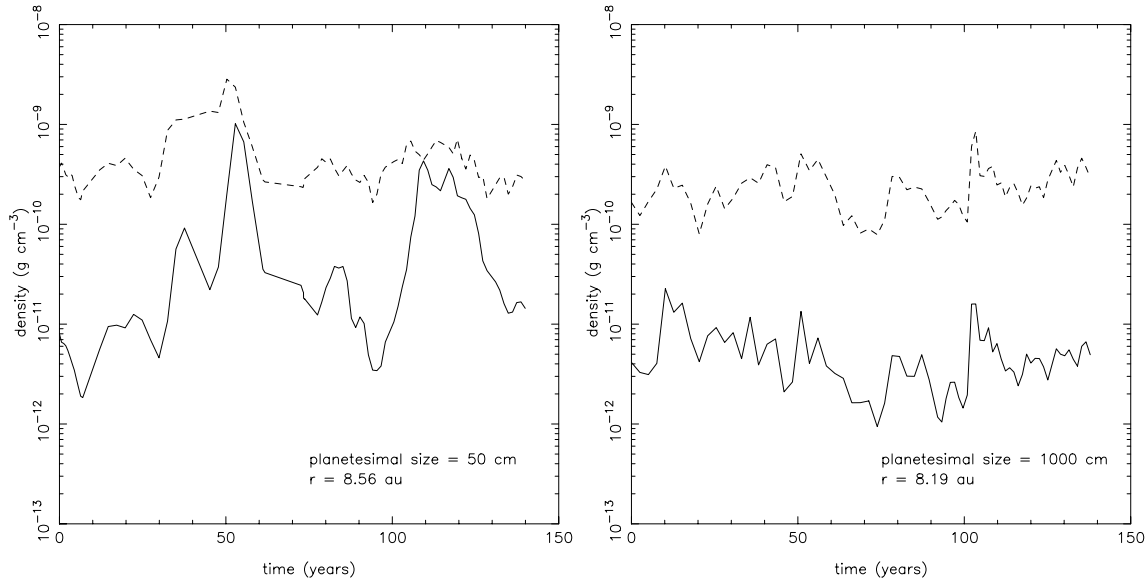
Figure 6. Time evolution of the densities for a 50-cm planetesimal (left panel) and for a 1000-cm planetesimal (right panel). The solid line shows the planetesimal density, while the dashed line shows the gas density.
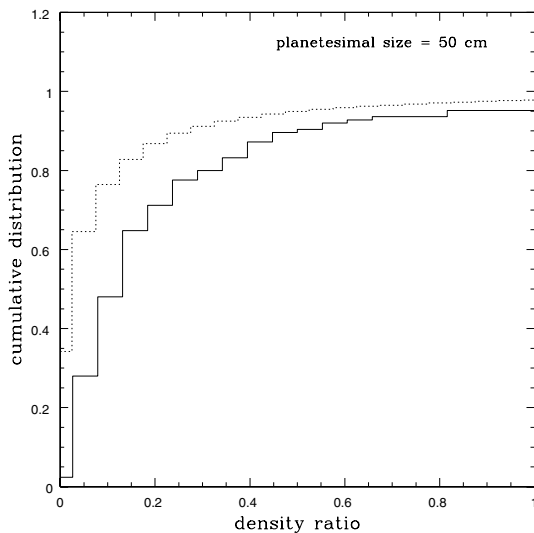

Figure 7. Solid line: cumulative distribution of the maximum of the density ratio ρ_p/ρ attained during the run. Dotted line: cumulative distribution of ρ_p/ρ at a given time. Both plots refer to the 50-cm case. While at any given time during the simulation the fraction of planetesimals with $\rho_p/\rho > 0.1$ (i.e. ρ_p/ρ enhanced by more than a factor 10) is ∼25 per cent, the fraction of planetesimal that at some stage during the simulation attains the same value of ρ_p/ρ is significantly higher, ∼75 per cent.

effect we have computed the maximum value of ρ_p/ρ attained by the planetesimals during the whole simulation (to reduce computational time, we have performed this analysis only for a subset of the total number of planetesimal SPH particles). The dotted line in Fig. 7 shows the cumulative distribution of ρ_p/ρ at a given time (i.e. the cumulative distribution corresponding to the solid line of Fig. 5), while the solid line shows the cumulative distribution of the maximum ρ_p/ρ, computed as described above. This figure clearly shows that, while at any given time during the simulation the fraction of planetesimals with $\rho_p/\rho > 0.1$ (i.e. ρ_p/ρ enhanced by more than a factor of 10) is ∼25 per cent, the fraction of planetesimal that

at some stage during the simulation attains the same value of ρ_p/ρ is significantly higher, ∼75 per cent.

5 DISCUSSION AND CONCLUSIONS

The concentration of planetesimals, owing to the combined effect of gas drag and gravity, that we find in our simulations can have a significant effect on the process of coagulation of planetesimals into larger bodies. This can occur either by increasing the planetesimal collision rate and/or by making the planetesimal subdisc gravitationally unstable.

The collision rate of planetesimals is proportional to $n_p\sigma_p$, where $n_p = \rho_p/m_p$ is the planetesimal number density and σ_p is their velocity dispersion. As in our case the Safronov number $\Theta = Gm_p/2\sigma_p^2 a$ is always much smaller than unity, we can neglect the effect of gravitational focusing. To assess the effect of gas drag on the collision rate, we have first computed the azimuthally averaged value of $n_p\sigma_p$ from the simulation with no drag force, $\langle n_p\sigma_p \rangle_{nd}$, as a function of radius. We have then computed, for every planetesimal SPH particle in both the 50-cm case and the 1000-cm case, the ratio $n_p\sigma_p/\langle n_p\sigma_p \rangle_{nd}$, where the average value is computed at the same radial location in the disc. If the gas drag had no effect on the collision rate, the distribution of $n_p\sigma_p/\langle n_p\sigma_p \rangle_{nd}$ would be strongly peaked around unity. Fig. 8 shows the distribution of $n_p\sigma_p/\langle n_p\sigma_p \rangle_{nd}$ that we have obtained in the three cases (no drag force: dashed line; 1000-cm size: dotted line; 50-cm size: solid line). As expected, the distribution for the no drag simulation is strongly peaked around unity. Fluctuations of $n_p\sigma_p$ not related to the gas drag result only in an increase of the collision rate by no more than a factor of ∼6. In contrast, the introduction of the gas drag leads to a broader distribution of collision rates, especially for the 50-cm case where the distribution has a tail extending more than two orders of magnitude above the average value. As discussed earlier, the fraction of particles concentrated in the spiral arms at a given time is smaller than the fraction of particles that, during the course of the whole simulation, are at some stage concentrated in the spiral arms. As the enhancement in collision rate is owing to the enhanced density
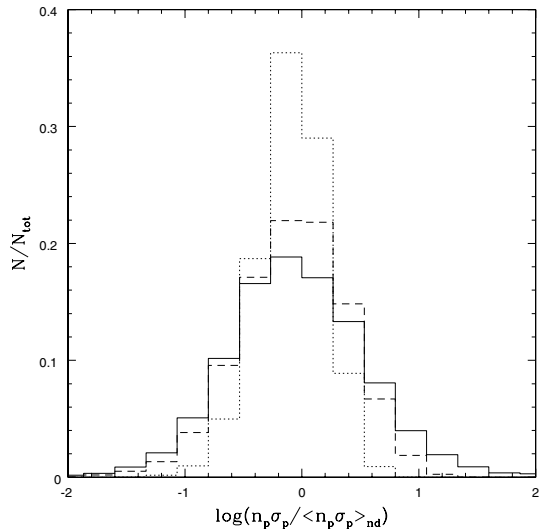
Figure 8. Distribution of $n_p\sigma_p/\langle n_p\sigma_p\rangle_{nd}$ for the 50-cm case (solid line), for the 1000-cm case (dashed line) and for the no drag simulation (dotted line). Fluctuations of $n_p\sigma_p$ not related to the gas drag result only in an increase of the collision rate by no more than a factor $\sim$6. In contrast, the introduction of the gas drag leads to a broader distribution of collision rates, especially for the 50-cm case, where the distribution has a tail extending up to two orders of magnitude above the average value.

resulting from the concentration of the planetesimals in the spiral arms, the number of particles over the entire simulation time that at some stage are in a region of enhanced collision rate will also be greater than the number at a single time. Depending on how well particles of this size stick together during collisions, this enhanced collision rate could play an important role in the growth of larger planetesimals.

A planetesimal surface density enhancement of a factor $\sim$20 may also be sufficient to make the planetesimal subdisc gravitationally unstable (e.g. Youdin & Shu 2002). This is exactly the range of concentrations that we achieve in the 50-cm simulation. However, as we have neglected the planetesimal self-gravity, we are not able

to obtain a gravitational instability in the planetesimal disc in our simulations (for a more detailed study of the stability of a two-component self-gravitating disc, see Bertin & Romeo (1988)). To assess the importance of the planetesimal self-gravity we have performed two separate tests.

We have first computed the quantity

$$\frac{\rho_p}{\bar{\rho}} = \frac{\rho_p R^3}{M_\star} = \frac{G\rho_p}{\Omega_K^2}, \tag{16}$$

where R is the radius of a region that has a local planetesimal density of ρ_p. This quantity is a measure of the relative effects of local gravitational collapse for the planetesimals versus tidal disruption. Fig. 9 shows the distribution of $\rho_p/\bar{\rho}$ in the 50-cm case (solid line) and in the 1000-cm case (dotted line). In the 50-cm case $\rho_p/\bar{\rho}$ reaches much higher values than in the 1000-cm case, becoming as large as $\sim$1. This suggests that the density enhancements in the 50-cm simulation may be gravitationally significant and that the planetesimal disc could become gravitationally unstable.

As a separate measure, we have also computed the Jeans mass, i.e.

$$M_J = \frac{1}{6}\pi\rho_p\left(\frac{\pi\sigma_p^2}{G\rho_p}\right)^{3/2}, \tag{17}$$

at the location of every planetesimal particle. If, at any location, the minimum resolvable mass (the mass, M, contained within two smoothing lengths) exceeds the local Jeans mass, then the self-gravity of the planetesimals has to play a role. The distribution of M/M_J is shown in the right panel of Fig. 9. In the 50-cm case, the distribution is shifted towards higher values and is much broader than in the 1000-cm case. For the most massive clumps, the ratio M/M_J can become comparable to or even larger than unity, indicating that the gravitational instability would play a significant role in these regions.

Note that as the vertical scaleheight of the planetesimal disc is comparable to the scaleheight of the gas disc, the high densities achieved in our simulation using 50-cm particles is only owing to radial and azimuthal compressions rather than by the vertical settling of the planetesimals in the midplane. Therefore, unlike in the standard picture for gravitational instability (Goldreich & Ward 1973;
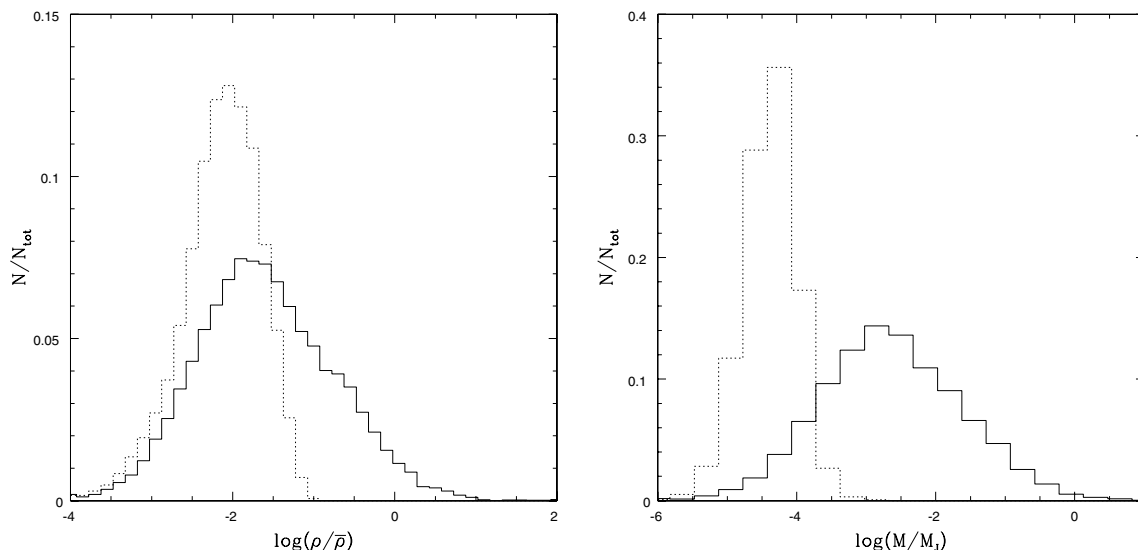

Figure 9. Left panel: distribution of $\rho_p/\bar{\rho}$ for the 50-cm (solid line) and the 1000-cm case (dotted line). Right panel: distribution of M/M_J in the two cases. These results show that some of the high-density clumps observed in the 50-cm case should be subject to gravitational instability.

Youdin & Shu 2002), our results should not be affected by additional turbulence generated by the vertical shear between the gas and the dust.

To summarize, in this work we have shown how the interaction between a self-gravitating gaseous protoplanetary disc and embedded planetesimals plays an important role in accelerating planetesimal growth. However, there are a number of important effects that we have neglected in this first approach to the problem as follows.

(i) The planetesimals have been essentially modelled as test particles, ignoring both the back reaction of the planetesimals on the gas and the planetesimal self-gravity. In regions where the planetesimal density is enhanced (becoming in some regions comparable to the gas density) both effects may be very important.

(ii) In each simulation the planetesimals are assumed to be of a single size and the volume density is computed by assuming that the initial surface density ratio is 0.01. In reality there will be a range of planetesimal sizes (e.g. Mathis, Rumpl & Nordsieck 1977; Mizuno, Markiewicz & Voelk 1988; note, however, that these studies consider grain sizes much smaller than those considered here) and only those with sizes, in this case, between $\sim$10 and 100 cm (see Fig. 1) will be significantly influenced by the self-gravitating structures in the gas disc. During the evolution of the protoplanetary nebula there might well be some stage where most of the planetesimal mass is contained within a relatively small range of sizes, so that our assumptions may not be unrealistic. When this size range includes the size for which the drift induced by the drag is significant, we can expect a significant increase in collision rate and an enhanced tendency toward gravitational collapse. To address the details of these processes we would need to consider many other effects (such as the sticking properties of planetesimals) which are beyond the scope of the present paper.

(iii) In this work we have considered, as an illustration, the self-gravitating structure resulting from a relatively massive gas disc (with a mass $\sim$0.25$M_\star$). However, a well-defined spiral structure is also present in significantly less massive discs (Lodato & Rice 2004). It would then be interesting to check the dependence of some of the details of the results described here (such as what is the relevant size range for the planetesimals that display the strongest response to the spiral structure) on the specific choice of the gas disc properties.

We plan in the future to include some of the effects described above, such as the backreaction of the planetesimals on the disc gas, the effect of planetesimal self-gravity, and we plan to consider various disc masses. However, it seems clear that if protoplanetary discs experience a self-gravitating phase, the resulting disc structures could well play an important role in planetesimal evolution and growth and could ultimately influence the growth of terrestrial planets and the cores of gas/ice giant planets. Also, as a protoplanetary disc is most likely to become gravitationally unstable early in the star formation process, we might expect substantial processing of the dust prior to the optically visible Classical T Tauri phase.

REFERENCES

Alibert Y., Mordasini C., Benz W., 2004, A&A, L25, 417
Bate M. R., Bonnell I. A., Price N. M., 1995, MNRAS, 277, 362
Benz W., 1990, in Buchler J., ed., The Numerical Modelling of Nonlinear Stellar Pulsations. Kluwer, Dordrecht, p. 269
Bertin G., Romeo A. B., 1988, A&A, 195, 105
Bodenheimer P., Hubickyj O., Lissauer J. J., 2000, Icarus, 143, 2
Boss A. P., 1998, Nat, 393, 141
Boss A. P., 2000, ApJ, 536, L101
Cuzzi J., Dobrovolski A. R., Champney J. M., 1993, Icarus, 106, 102
Gammie C. F., 2001, ApJ, 553, 174
Garaud P., Barriére-Fouchet L., Lin D. N. C., 2004, ApJ, 603, 292
Godon P., Livio M., 2000, ApJ, 537, 396
Goldreich P., Ward W. R., 1973, ApJ, 183, 105
Haghighipour N., Boss A. P., 2003a, ApJ, 583, 996
Haghighipour N., Boss A. P., 2003b, ApJ, 598, 1301
Haisch K., Lada E., Lada C., 2001, ApJ, 552, L153
Hourigan K., Ward W. R., 1984, Icarus, 60, 29
Johnson B. M., Gammie C. F., 2003, ApJ, 597, 131
Klahr H., Bodenheimer P., 2003, in Fridlund M., Henning T., eds, ESA Spec. Pub. SP-539, DARWIN/TPF and the Search for Extrasolar Terrestrial Planets. ESA Publications, Heidelberg, p. 481
Lin D. N. C., Pringle J. E., 1990, ApJ, 358, 515
Lissauer J. J., 1993, ARA&A, 31, 129
Lodato G., Bertin G., 2001, A&A, 375, 455
Lodato G., Rice W. K. M., 2004, MNRAS, 351, 630
Mathis J. S., Rumpl W., Nordsieck K. H., 1977, ApJ, 217, 425
Mizuno H., Markiewicz W. J., Voelk H. J., 1988, A&A, 195, 183
Monaghan J. J., 1992, ARA&A, 30, 543
Nelson R. P., Papaloizou J. C. B., 2004, MNRAS, 350, 849
Pickett B. K., Cassen P., Durisen R. H., Link R., 1998, ApJ, 504, 468
Pickett B. K., Cassen P., Durisen R. H., Link R., 2000, ApJ, 529, 1034
Pollack J. B., Hubickyj O., Bodenheimer P., Lissauer J. J., Podolak M., Greenzweig Y., 1996, Icarus, 124, 62
Rice W. K. M., Armitage P. J., 2003, ApJ, 598, L55
Rice W. K. M., Armitage P. J., Bate M. R., Bonnell I. A., 2003a, MNRAS, 338, 227
Rice W. K. M., Armitage P. J., Bate M. R., Bonnell I. A., Jeffers S. V., Vine S. G., 2003b, MNRAS, 346, L36
Safronov V. S., 1972, Evolution of the Protoplanetary Cloud and Formation of the Earth and the Planets. Israel Program of Science Translation, Jerusalem
Stone J. M., Hawley J. F., Gammie C. F., Balbus S. A., 1996, ApJ, 463, 656
Supulver K. D., Lin D. N. C., 2000, Icarus, 146, 525
Takeuchi T., Lin D. N. C., 2002, ApJ, 581, 1344
Toomre A., 1964, ApJ, 139, 1217
Weidenschilling S., 1977, MNRAS, 180, 57
Weidenschilling S. J., Cuzzi J. N., 1993, in Levy E. H., Lunine J. I., eds, Protostars and Planets III. University of Arizona Press, Tucson, p. 1031
Wetherill G., 1990, ARE&PS, 18, 205
Whipple F. L., 1972, in Elvius A., ed., From Plasma to Planets. Wiley, London, p. 211
Youdin A. N., Chiang E. I., 2004, ApJ, 601, 1109
Youdin A. N., Shu F. H., 2002, ApJ, 580, 494

This paper has been typeset from a TEX/LATEX file prepared by the author.